Uncertainties in modeling low-energy neutrino-induced reactions on iron-group nuclei

Paar, Nils; Suzuki, Toshio; Honma, M.; Marketin, Tomislav; Vretenar, Dario

Uncertainties in modeling low-energy neutrino-induced reactions on iron-group nuclei

N. Paar,[1] T. Suzuki,[2] M. Honma,[3] T. Marketin,[1,4] and D. Vretenar[1]
[1]*Physics Department, Faculty of Science, University of Zagreb, Croatia*
[2]*Department of Physics, College of Humanities and Sciences, Nihon University, Sakurajosui 3-25-40, Setagaya-ku, Tokyo 156-8550, Japan*
[3]*Center for Mathematical Sciences, University of Aizu, Aizu-Wakamatsu, Fukushima 965-8580, Japan*
[4]*GSI Helmholtzzentrum für Schwerionenforschung, Planckstraße 1, D-64291 Darmstadt, Germany*
(Received 1 September 2011; published 31 October 2011)

Charged-current neutrino-nucleus cross sections for ^{54,56}Fe and ^{58,60}Ni are calculated and compared using frameworks based on relativistic and Skyrme energy-density functionals and on the shell model. The current theoretical uncertainties in modeling neutrino-nucleus cross sections are assessed in relation to the predicted Gamow-Teller transition strength and available data, to multipole decomposition of the cross sections, and to cross sections averaged over the Michel flux and Fermi-Dirac distribution. By employing different microscopic approaches and models, the decay-at-rest (DAR) neutrino-^{56}Fe cross section and its theoretical uncertainty are estimated to be $\langle\sigma\rangle_{\rm th} = (258 \pm 57) \times 10^{-42}$ cm^2, in very good agreement with the experimental value $\langle\sigma\rangle_{\rm exp} = (256 \pm 108 \pm 43) \times 10^{-42}$ cm^2.

DOI: 10.1103/PhysRevC.84.047305 PACS number(s): 21.30.Fe, 21.60.Jz, 23.40.Bw, 25.30.−c

Weak neutrino-induced processes in nuclei provide information of relevance for modeling responses in neutrino detectors, understanding fundamental properties of the weak interaction, and determining the role of neutrinos in stellar environments. Data on neutrino-nucleus cross sections are presently available only for ^{12}C and ^{56}Fe target nuclei; they were obtained by the Liquid Scintillator Neutrino Detector (LSND) [1], the Karlsruhe-Rutherford Medium-Energy Neutrino Experiment (KARMEN) [2,3], and at the Los Alamos Meson Physics Facility (LAMPF) [4]. At present only theoretical approaches can provide cross sections for a large number of target nuclei that are involved in various applications of neutrino physics and astrophysics. It is therefore crucial to quantitatively assess the theoretical uncertainties in modeling neutrino-induced processes, including the detailed structure of principal transitions and the total cross sections averaged over selected neutrino fluxes. The evaluation of current theoretical uncertainties in modeling neutrino-induced processes is also important in view of future experimental programs, e.g., the Spallation Neutron Source (SNS) at Oak Ridge National Laboratory [5], the Large Volume Detector (LVD) at Gran Sasso National Laboratory [6], and the production of neutrinos using β decay of boosted radioactive ions [7,8].

Over the years a variety of microscopic models have been developed and employed in the calculation of neutrino-nucleus cross sections at low energies. These include the shell model [9–13], the random-phase approximation (RPA) [12,14,15], continuum RPA (CRPA) [16–18], hybrid models of CRPA and the shell model [14,19], the Fermi gas model [20], quasiparticle RPA (QRPA) [21,22], projected QRPA [23], and relativistic quasiparticle RPA (RQRPA) [24]. For the purpose of the present analysis of theoretical uncertainties in modeling neutrino-nucleus cross sections we chose the iron-group nuclei. For these nuclei, frameworks based on energy-density functionals and the shell model represent feasible approaches and, in addition, data from muon decay at rest (DAR) are available [2,3]. The framework based on energy-density functionals employs the relativistic Hartree-Bogoliubov (RHB) model to determine the nuclear ground state and the RQRPA to calculate all relevant transitions induced by the incoming neutrinos [24]. Model calculations are performed using effective interactions with density-dependent meson-nucleon couplings—in this case the DD-ME2 interaction [25]—whereas pairing correlations are described by the finite-range Gogny force [26]. The nuclear shell model employed in the present study is based on the GXPF1J effective interaction [27] for the $\lambda^\pi = 1^+$ channel, supplemented by the RPA based on a Skyrme functional (SGII) for other multipoles [13]. A detailed analysis of (anti)neutrino-^{56}Fe cross sections based on the QRPA with Skyrme functionals is given in Ref. [21]. Shell-model calculations are carried out with the code MSHELL [28].

Because of its importance for neutrino-nucleus cross sections at low energies, we start by analyzing the Gamow-Teller (GT) transition strength B in the iron-group nuclei. Figure 1 displays the GT$^-$ strength distributions for ^{56}Fe, obtained using the shell model (GXPF1J) and the RQRPA (DD-ME2). In both cases the calculated transition strength is folded by a Lorentzian with a width of $\Gamma = 0.5$ MeV. The RQRPA includes only $2qp$ configurations and therefore cannot provide the detailed structure of excitation spectra obtained by the shell model. Nevertheless, one can observe that the calculated transition-strength distributions are in reasonable agreement.

In Figs. 2 and 3 the GT$^\pm$ transition strengths contributing to the neutrino-induced processes are compared for a set of iron-group nuclei: ^{54,56}Fe and ^{58,60}Ni. The following models and respective parametrizations have been used: (i) the RPA based on Skyrme functionals (SGII, SLy5), (ii) the RQRPA (DD-ME2) [25], and (iii) the shell model (GXPF1J) [13]. Results of model calculations are compared with the data for GT$^-$ [29] and GT$^+$ [30–32] transition strengths. The (Q)RPA calculations include the quenching of the free-nucleon axial-vector coupling constant $g_A = 1.262 \rightarrow g_A = 1$, corresponding to a quenching factor of 0.8 in the

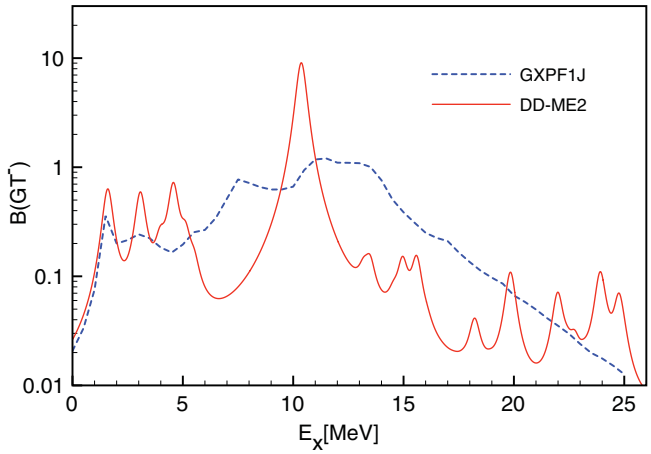

FIG. 1. (Color online) GT$^-$ transition strength in ^{56}Fe, calculated using the RQRPA (DD-ME2) and the shell model (GXPF1J).

GT transition operator. A quenching factor is also used in the shell model. However, its value of 0.74 is adapted to the effective interaction and model space under consideration [13]. One notices in Figs. 2 and 3 that the shell model reproduces the experimental values of GT$^-$ transition strength with high accuracy (except for ^{60}Ni), and also that the GT$^+$ strength is reasonably reproduced. (Q)RPA-based approaches, however, even by quenching the value $g_A \to 1$, overestimate both the GT$^-$ and GT$^+$ transition strengths. For ^{54,56}Fe and ^{58}Ni the relativistic QRPA results for B_{GT^-} are within experimental uncertainties. The fact that the QRPA calculations systematically overestimate the measured GT$^\pm$ transition strength, even though different effective interactions are used, indicates that a somewhat stronger quenching of the axial-vector coupling constant might be necessary to reproduce the data. Actually, if the same quenching factor of 0.74 used by the shell model is also employed in (Q)RPA calculations, a very good agreement with the shell-model results is obtained. The (Q)RPA and shell-model B_{GT^-} values, all obtained using the same quenching factor 0.74, are shown in Table I in comparison to the data [29]. In this case, for all four nuclei ^{54,56}Fe and ^{58,60}Ni, the (Q)RPA B_{GT^-} values are found to be in good agreement with the shell-model results, particularly for the relativistic QRPA (DD-ME2). We have verified that the same result is also obtained for the B_{GT^+} channel. This similarity is not obvious, as the two theoretical frameworks have different foundations and use different effective interactions and model spaces. One should consider this result with caution because of the well-known problem of missing GT strength, due either to excitations that involve complex configurations at higher excitation energies or to excitations that include non-nucleonic degrees of freedom.

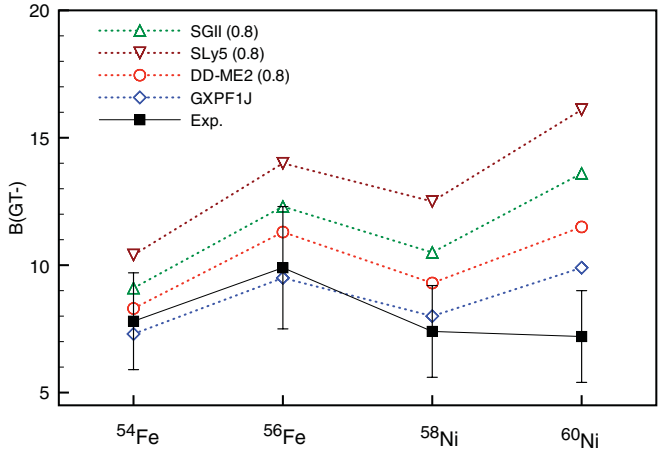

FIG. 2. (Color online) GT$^-$ transition strengths calculated with the Skyrme RPA (SGII, SLy5) and the RQRPA (DD-ME2), in comparison to the shell model (GXPF1J) [13] and experimental values [29]. (Q)RPA calculations include a quenching factor of 0.8 in the axial-vector coupling constant g_A.

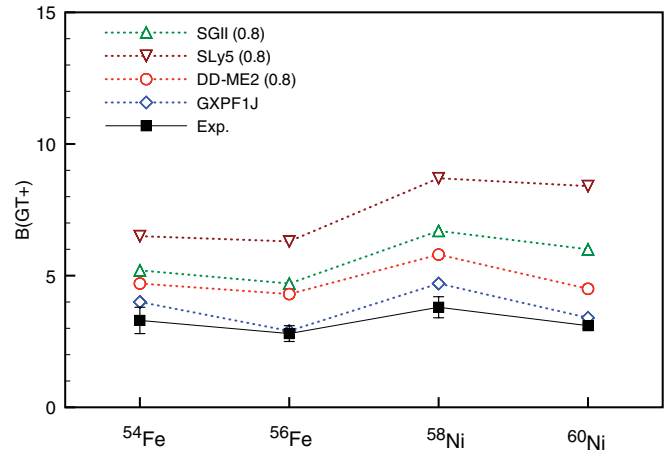

FIG. 3. (Color online) Same as described in the caption to Fig. 2 but for the GT$^+$ transitions. Experimental values are from Refs. [30–32].

As already emphasized in previous studies of neutrino-nucleus reactions [21,24], not only GT$^-$ transitions but also excitations of higher multipoles must be included, depending on the energy range under consideration. In this work we analyze the reaction ^{56}Fe$(\nu_e, e^-)^{56}$Co in more detail, using two representative theoretical approaches: the shell model (GXPF1J), supplemented by the RPA based on Skyrme functionals (SGII), and the fully consistent relativistic framework RHB + QRPA (DD-ME2). The goal is to provide an estimate of theoretical uncertainties of contributions from different multipole transitions to the neutrino cross section. In Fig. 4 we plot the contributions of the multipole transitions $\lambda^\pi = 0^\pm$–$4^\pm$ to the inclusive cross section for the

TABLE I. GT$^-$ transition strengths calculated using the Skyrme RPA (SGII, SLy5), RQRPA (DD-ME2), and shell model (GXPF1J) [13] (all using $g_A^* = 0.74 g_A$), compared to experimental values [29].

	^{54}Fe	^{56}Fe	^{58}Ni	^{60}Ni
SGII	7.8	10.5	9.0	11.7
SLy5	8.9	11.9	10.7	13.8
DD-ME2	7.1	9.7	7.9	9.8
GXPF1J	7.3	9.5	8.0	9.9
Expt.	7.8 ± 1.9	9.9 ± 2.4	7.4 ± 1.8	7.2 ± 1.8

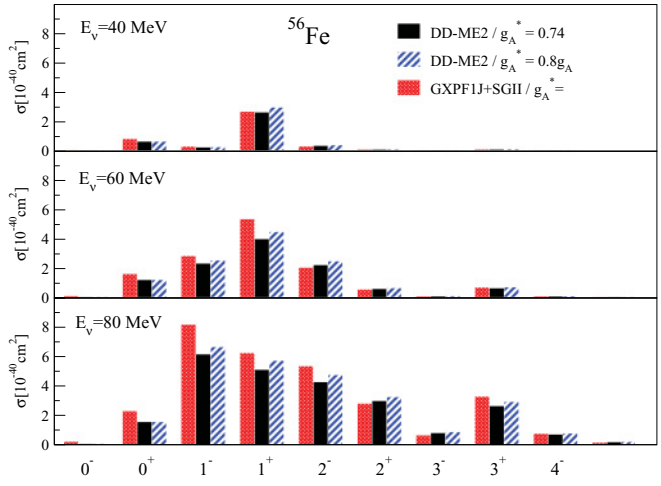

FIG. 4. (Color online) Contributions of the multipole transitions $\lambda^\pi = 0^\pm$–$4^\pm$ to the inclusive cross section for the ^{56}Fe$(\nu_e, e^-)^{56}$Co reaction, at $E_{\nu_e} = 40$, 60, and 807nbsp;MeV. Calculations include RHB + RQRPA (DD-ME2) and the shell model (GXPF1J) (for the 1^+ transition) plus the RPA (SGII) for higher multipoles. The quenching factors in g_A are denoted in the figure.

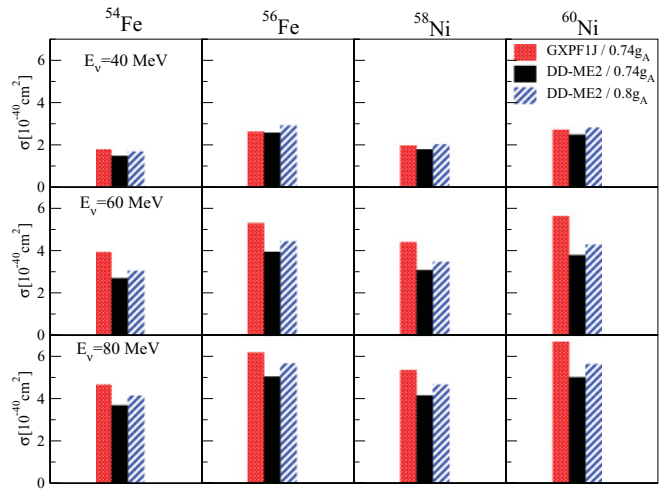

FIG. 5. (Color online) Inclusive neutrino-nucleus cross sections in the 1^+ channel for the ^{54,56}Fe and ^{58,60}Ni target nuclei, at incoming neutrino energies $E_{\nu_e} = 40$, 60, and 80 MeV. The results are obtained using the RHB + RQRPA (DD-ME2) framework and the shell model (GXPF1J). The axial-vector coupling g_A^* includes a quenching factor as denoted in the figure.

^{56}Fe$(\nu_e, e^-)^{56}$Co reaction, at $E_{\nu_e} = 40$, 60, and 80 MeV. The RHB + RQRPA (DD-ME2) calculations include the standard (0.8) and enhanced (0.74) quenching factors of the axial-vector coupling constant g_A in all multipole operators. In the nonrelativistic framework, the shell model (GXPF1J) is used for 1^+ transitions and the RPA (SGII) is used for higher multipoles. The quenching factor for the axial-vector coupling g_A is 0.74. In the shell-model calculation of 1^+ transitions the effect of finite momentum transfer (q) is taken into account by evaluating the matrix elements $\langle f||j_0(qr)[Y^0 \times \vec{\sigma}]^1 t_-||i\rangle$ and $\langle f||j_2(qr)[Y^2 \times \vec{\sigma}]^1 t_-||i\rangle$ at each q, instead of the approximate treatment used in Ref. [13] where the GT matrix element $\langle f||j_0(qR)\vec{\sigma}t_-||i\rangle$ was evaluated with multiplier $j_0(qR)$ (where R is the nuclear radius).

At relatively low neutrino energies ($E_\nu \lesssim 40$ MeV) the dominant contribution to the calculated cross sections originates from GT transitions ($\lambda^\pi = 1^+$). With increasing E_ν, however, contributions from other multipole transitions become important. In particular, at $E_\nu = 80$ MeV the dominant transition is the spin dipole $\lambda^\pi = 1^-$; but other components, e.g., $\lambda^\pi = 1^+$, 2^-, 2^+, and 3^+, also play an important role. The cross sections plotted in Fig. 4 show that the two models predict a very similar structure and distribution of the relative contributions from various multipoles. These results are also in agreement with those discussed in Ref. [21].

In Fig. 5 we compare the neutrino-capture cross sections for the λ^π=1^+ channel on the set of target nuclei ^{54,56}Fe and ^{58,60}Ni for incoming neutrino energies $E_{\nu_e} = 40$, 60, and 80 MeV. The results are obtained using the RHB + RQRPA (DD-ME2) and the shell model (GXPF1J). The axial-vector coupling g_A^* includes a quenching factor as denoted in the figure. The cross sections increase in heavier isotopes because electron neutrinos are captured by neutrons. The two models, although based on different microscopic pictures, predict rather similar cross sections. One notes that at higher neutrino energies the shell- model cross sections are slightly larger than those calculated with the RQRPA. Compared to the previous discussion of the overall GT strength and the quenching of g_A, from the cross sections shown in Fig. 5 it appears that the (Q)RPA does not require a stronger quenching than the usual $g_A = 1$ to be in agreement with the shell model. The reason is that the calculated cross sections are determined not only by the overall GT transition strength but also by the transition energies that govern the energies of outgoing electrons.

We have also analyzed cross sections averaged over the neutrino flux described by the Fermi-Dirac spectrum [24]. Figure 6 displays the flux-averaged cross sections for the reaction ^{56}Fe$(\nu_e, e^-)^{56}$Co, evaluated at different temperatures in the interval $T = 2$–10 MeV, and for the chemical potential $\alpha = 0$. The RHB + RQRPA (DD-ME2) calculations including the standard (0.8) and enhanced (0.74) quenching factors in g_A are compared to the shell- model + RPA (GXPF1J + SGII) results [13] and to those obtained using a hybrid model in Ref. [33]. The latter model predicts somewhat larger cross sections, whereas a very good agreement is found between the results of the shell model + RPA and the RQRPA.

The theoretical cross sections for the reaction ^{56}Fe$(\nu_e, e^-)^{56}$Co can also be analyzed in comparison to data from the KARMEN Collaboration. The calculated cross sections are averaged over the neutrino flux described by the Michel spectrum obtained from muon decay at rest: $f(E_{\nu_e}) = (96E_{\nu_e}^2/m_\mu^4)(m_\mu - 2E_{\nu_e})$. By taking into account the results obtained in this work with the RHB + RQRPA (DD-ME2) (263×10^{-42} cm^2) and with the shell model (GXPF1J) for 1^+ transitions plus the RPA (SGII) for other multipoles (259×10^{-42} cm^2), as well as results from previous studies that used the RPA with a Landau-Migdal force (240×10^{-42} cm^2 [33]), the QRPA (SIII) (352×10^{-42} cm^2 [21]), and the QRPA based on G-matrix formalism (173.5×10^{-42} cm^2 [22]), the DAR neutrino-nucleus cross

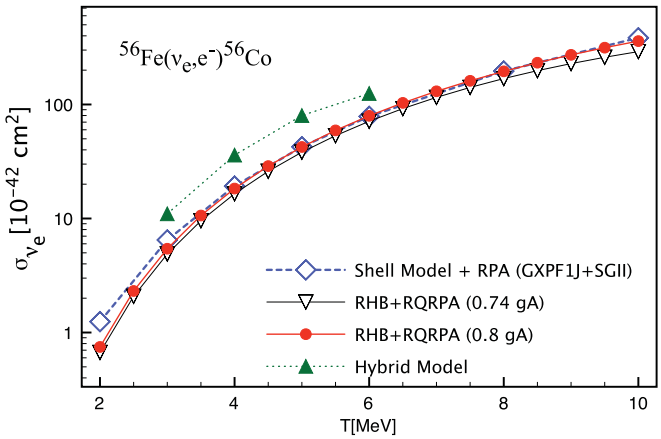

FIG. 6. (Color online) Neutrino-^{56}Fe cross sections averaged over the Fermi-Dirac distribution. The RHB+RQRPA (DD-ME2) calculations, including the standard (0.8) and enhanced (0.74) quenching factors of the axial-vector coupling g_A, are compared to shell-model + RPA results [13] and to those obtained using a hybrid model [33].

section and its theoretical uncertainty are estimated to be $\langle\sigma\rangle_{\rm th} = (258 \pm 57) \times 10^{-42}$ cm^2. This value is in very good agreement with the data from the KARMEN Collaboration: $\langle\sigma\rangle_{\rm exp} = (256 \pm 108 \pm 43) \times 10^{-42}$ cm^2. We note that the various models used to obtain the theoretical estimate employ different effective interactions and also comprise a wide range of values for the axial-vector coupling: from those without quenching [21,22] to models that use a quenching factor of 0.7 [33]. All of the theory frameworks, except the QRPA based on the G-matrix formalism, favor the quenching of the axial-vector coupling constant g_A in accordance with constraints given by the experimental data on Gamow-Teller transitions. The implementation of the quenching of g_A in the QRPA based on Skyrme functionals [21] would lower the calculated neutrino-nucleus cross sections and it would further reduce the overall theoretical uncertainty in $\langle\sigma\rangle_{\rm th}$.

In conclusion, the charged current neutrino-nucleus cross sections for ^{54,56}Fe and ^{58,60}Ni have been analyzed by employing models based on the relativistic and Skyrme energy-density functionals and on the shell model. The theoretical uncertainties in modeling neutrino-induced processes have been examined by considering the Gamow-Teller transition strength and available data, the multipole decomposition of the calculated cross sections, and cross sections averaged over the Michel flux and Fermi-Dirac distribution. It has been shown that various models predict very similar multipole distributions of neutrino-nucleus cross sections. The corresponding cross sections averaged over the DAR neutrino spectra show that the current theoretical uncertainty, despite a variety of models and effective interactions that have been used in many studies, is actually smaller than the experimental one and could be even further reduced by constraining the quenching of the axial-vector coupling constant g_A to data for the Gamow-Teller transition strength.

This work is supported by the Croatian Ministry of Science, Education and Sports (MZOS) under Grant No. 1191005-1010, by the Croatian Science Foundation, and by the Ministry of Education, Culture, Sports, Science and Technology in Japan (MEXT), under Grant-in-Aid for Scientific Research No. (C) 22540290.

[1] C. Athanassopoulos *et al.*, Phys. Rev. C **55**, 2078 (1997).
[2] B. E. Bodmann *et al.*, Phys. Lett. B **332**, 251 (1994).
[3] R. Maschuw, Prog. Part. Nucl. Phys. **40**, 183 (1998).
[4] D. A. Krakauer *et al.*, Phys. Rev. C **45**, 2450 (1992).
[5] F. T. Avignone, L. Chatterjee, Yu. V. Efremenko, and M. Strayer, J. Phys. G **29**, 2497 (2003).
[6] N. Yu. Agafonova *et al.*, Astron. Phys. **27**, 254 (2007).
[7] P. Zucchelli, Phys. Lett. B **532**, 166 (2002).
[8] C. Volpe, J. Phys. G **30**, L1 (2004).
[9] W. C. Haxton, Phys. Rev. D **36**, 2283 (1987).
[10] J. Engel, E. Kolbe, K. Langanke, and P. Vogel, Phys. Rev. C **54**, 2740 (1996).
[11] A. C. Hayes and I. S. Towner, Phys. Rev. C **61**, 044603 (2000).
[12] C. Volpe, N. Auerbach, G. Colò, T. Suzuki, and N. Van Giai, Phys. Rev. C **62**, 015501 (2000).
[13] T. Suzuki, M. Honma, K. Higashiyama, T. Yoshida, T. Kajino, T. Otsuka, H. Umeda, and K. Nomoto, Phys. Rev. C **79**, 061603(R) (2009).
[14] N. Auerbach, N. Van Giai, and O. K. Vorov, Phys. Rev. C **56**, R2368 (1997).
[15] S. K. Singh, N. C. Mukhopadhyay, and E. Oset, Phys. Rev. C **57**, 2687 (1998).
[16] E. Kolbe, K. Langanke, S. Krewald, and F.-K. Thielemann, Nucl. Phys. A **540**, 599 (1992).
[17] N. Jachowicz, S. Rombouts, K. Heyde, and J. Ryckebusch, Phys. Rev. C **59**, 3246 (1999).
[18] A. Botrugno and G. Co', Nucl. Phys. A **761**, 200 (2005).
[19] E. Kolbe, K. Langanke, and G. Martínez-Pinedo, Phys. Rev. C **60**, 052801 (1999).
[20] T. Kuramoto, M. Fukugita, Y. Kohyama, and K. Kubodera, Nucl. Phys. A **512**, 711 (1990).
[21] R. Lazauskas and C. Volpe, Nucl. Phys. A **792**, 219 (2007).
[22] M. K. Cheoun, E. Ha, K. S. Kim, and T. Kajino, J. Phys. G **37**, 055101 (2010).
[23] A. R. Samana, F. Krmpotić, N. Paar, and C. A. Bertulani, Phys. Rev. C **83**, 024303 (2011).
[24] N. Paar, D. Vretenar, T. Marketin, and P. Ring, Phys. Rev. C **77**, 024608 (2008).
[25] G. A. Lalazissis, T. Nikšić, D. Vretenar, and P. Ring, Phys. Rev. C **71**, 024312 (2005).
[26] J. F. Berger, M. Girod, and D. Gogny, Comput. Phys. Commun. **63**, 365 (1991).
[27] M. Honma, T. Otsuka, T. Mizusaki, M. Hjorth-Jensen, and B. A. Brown, J. Phys.: Conf. Ser. **20**, 7 (2005).
[28] T. Mizusaki, RIKEN Accel. Prog. Rep. **33**, 14 (2000).
[29] J. Rapaport *et al.*, Nucl. Phys. A **410**, 371 (1983).
[30] M. C. Vetterli *et al.*, Phys. Rev. C **40**, 559 (1989).
[31] S. El-Kateb *et al.*, Phys. Rev. C **49**, 3128 (1994).
[32] A. L. Williams *et al.*, Phys. Rev. C **51**, 1144 (1995).
[33] E. Kolbe and K. Langanke, Phys. Rev. C **63**, 025802 (2001).